Why Does the Amazon Water Flow to the North after Its Discharge?*

HSIEN WANG OU

Lamont-Doherty Geological Observatory of Columbia University, Palisades, New York

(Manuscript received 22 September 1988, in final form 15 March 1989)

ABSTRACT

Through a simple model, it is demonstrated that earth's sphericity (the beta effect) imposes a severe constraint on the discharge pattern near the equator. Using either bottom or lateral friction to counter the beta effect in the vorticity balance, the flow in the far field is confined to boundary layers either along the solid boundaries that are open on the anticyclonic side or along the equator to the west of the point source. Thus, for all possible orientation of the radial boundaries flanking the point source, there are either one or two branches receptive of the discharge in the far field depending on whether the open angle spanned by the two boundaries excludes the east direction. Even when the branching is permissible, it is further argued, based on symmetry of the governing equation, that the outflow is strongly favored toward the branch that deviates more from the east direction. Numerical solutions show that the bulk of the diversion of the discharge to this branch occurs within one frictional scale of the point source. Since this distance, as crudely estimated, can be of order 100 km, the model can explain the sharp deflection of the Amazon outflow to the northern coast over the shelf proper without requiring asymmetric external forcings.

1. Introduction

Observations show that the Amazon water, after its discharge near the equator, turns sharply to the northern coast (Muller-Karger et al. 1988), with its freshening effect detected as far north as the Carribbean Sea (Borstad 1982). Although one can speculate upon the effects of regional wind and offshore North Brazil Current, both of which are directed toward the north, whether they are of sufficient magnitude to cause the observed deflection has not been determined. In this paper, I shall instead offer an alternative explanation based on internal constraint imposed by the beta effect rather than asymmetric external forcings. As demonstrated by a simple model that, because the coastline is not strictly north–south oriented, the Amazon outflow should deflect sharply to the northern coast within one frictional scale of the order 100 km, consistent with observations.

2. The model

Let us consider a point source at the equator discharging water into an open domain flanked by two radial boundaries, as schematically shown in Fig. 1. For simplicity, we assume the flow to be nondivergent and hence can be represented by a streamfunction. One should be cautioned however that vortex stretching associated with horizontal divergence is pivotal in controlling the outflow dispersal in midlatitudes. The effect however is of reduced importance here because of vanishing Coriolis parameter and hence is neglected. We shall first consider the case of bottom friction which, because of the large tidal currents observed in the region (Gibbs 1982), is likely to be the dominant dissipative mechanism. The use of lateral friction will be discussed in the next section which does not alter the main conclusions using the simpler bottom friction.

Let us assume a vorticity balance between the beta effect and bottom friction, so that

$$\beta\psi_x = -\alpha\nabla^2\psi, \tag{2.1}$$

where ψ is the streamfunction, β the planetary vorticity gradient and α the resistence coefficient defined as C_dU/H with C_d being the drag coefficient, U the amplitude of the tidal current and H the water depth. Partial derivatives are denoted by subscripts. If we nondimensionalize ψ by the discharge rate and distance by α/β, then (2.1) can be written in the polar coordinate as

$$\nabla^2\psi + \cos\theta\psi_r - r^{-1}\sin\theta\psi_\theta = 0, \tag{2.2}$$

where $\nabla^2 \equiv r^{-1}\partial_r r\partial_r + r^{-2}\partial_\theta{}^2$. The boundary conditions are that $\psi = 1$ at $\theta = \theta_1$, $\psi = 0$ at $\theta = \theta_2$ and the solution be well behaved as r approaches zero or infinity.

In the near field ($r \ll 1$) where the beta terms are small compared with the friction term, (2.2) has the solution

---

* Lamont-Doherty Geological Observatory Contribution Number 000.

Corresponding author address: Dr. Hsien Wang Ou, Lamont-Doherty Geological Observatory of Columbia University, Palisades, NY 10964.

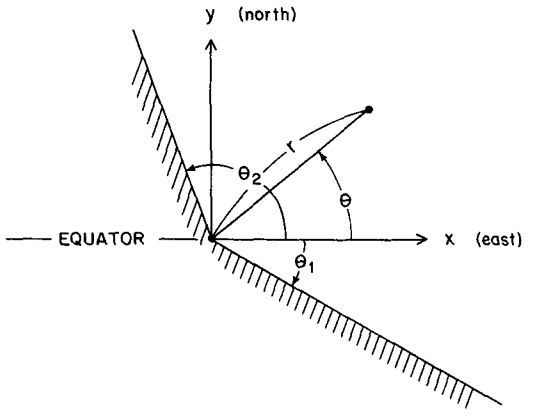

FIG. 1. Model configuration by which a point source located at the equator discharges water into an open domain flanked by two radial boundaries.

$$\psi = \frac{\theta_2 - \theta}{\theta_2 - \theta_1}, \tag{2.3}$$

which represents a uniform radial flow emanating from the point source. As r increases, the beta effect disturbs this radial pattern by inducing anticyclonic vorticity on both sides of the equator. In the far field ($r \gg 1$), since the beta terms decrease with r at a slower rate (as r^{-1}) than the friction term (as r^{-2}), they must become important and the flow is increasingly confined to the boundary layer where the dominant balance is between the bottom drag acting on the cross-stream shear and the beta terms, or

$$r^{-2}\psi_{\theta\theta} + \cos\theta\psi_r - r^{-1}\sin\theta\psi_\theta \approx 0. \tag{2.4}$$

Let θ_b be the azimuthal angle of the boundary and θ' ($\equiv\theta - \theta_b$) characterizing the angular spread of the boundary layer, one can derive from (2.4) the scaling dependence of θ' on r which, as we shall see below, is different for zonal and nonzonal boundaries.

For a nonzonal boundary ($\sin\theta_b \neq 0$), (2.4) implies that θ' scales as r^{-1} and the balance is between the first and third term or, in terms of the similarity variable η ($\equiv r\theta'\sin\theta_b$),

$$\psi_{\eta\eta} - \psi_\eta = 0. \tag{2.5}$$

The solution ($\psi_\eta = Ce^\eta$) decays only for negative η and hence the boundary layer is permissible only on the anticyclonic side of the boundary. This is thus a trivial extension of Stommel's boundary layer (1948) to nonmeridional boundaries. The width of the boundary layer, given by the e-folding scale $|\eta| = 1$ or $|r\theta'| = |\sin\theta_b|^{-1}$, is a constant in r, which is greater for a more zonally oriented boundary. This is expected as beta effect diminishes for such boundaries.

Based on this result that a boundary layer is permissible only on the anticyclonic side of a nonzonal boundary, one deduces by extrapolation that as the boundary becomes zonal (i.e. along the equator), a boundary layer is permissible only if it is directed to the west (since both sides of the boundary are anticyclonic), but not when it is directed to the east (both sides are cyclonic). Since $\sin\theta_b = 0$ for a zonal boundary, the boundary-layer scaling leading to (2.5) breaks down, one needs to consider the next terms in the series expansion of $\sin\theta$ in (2.4). Setting $\sin\theta$ to be $\mp\theta'$ in the far field (the upper and lower signs are for boundaries directing to the west and east respectively), (2.4) implies that $|\theta'|$ decreases as $r^{-1/2}$, a slower rate than that for a nonzonal boundary. The ψ_r term in (2.4) however can no longer be neglected as it varies with r^{-1}, the same rate as the other terms. Defining the similarity variable η as $\theta' r^{1/2}$, then in the new coordinate system (r, η), the similarity solution $\psi = \psi(\eta)$ satisfies the equation,

$$\psi_{\eta\eta} \pm \frac{1}{2}\eta\psi_\eta = 0. \tag{2.6}$$

The equation has a solution decaying with $|\eta|$ ($\psi_\eta = Ce^{-\eta 2/4}$) only if the upper sign is chosen or, as reasoned above, the boundary current is directed toward the west. The width of the boundary layer, as given by the e-folding scale $|\eta| = 2$ or $|r\theta'| = 2r^{1/2}$, is no longer constant but increases downstream. Physically, the frictional torque acting on a westward flow (which has an anticyclonic vorticity) must be balanced by an increase in planetary vorticity and, along a zonal boundary, this can be achieved only through a widening current.

Since one notes from (2.6) that the current shear vanishes at the equator, the solution can be extended smoothly across the equator to form a free symmetric jet. Thus, in addition to the solid boundaries when they are open on the anticyclonic side, the equator to the west of the point source provides an additional virtual boundary for the presence of a boundary current. Based on this criteria, one can easily infer that for all different orientation of the two radial boundaries flanking the point source, there are only four possible arrangements of the boundary current, depending on the relation between the open angle (spanned by the radial boundaries) and the east and west directions. Examples of the four possible cases are plotted schematically in Fig. 2. In cases I and II when this open angle excludes the east direction, there is only one boundary current permissible. It is along a solid boundary if the west direction is also excluded, otherwise it is along the equator to the west. In cases III and IV when this open angle encompasses the east direction, there are two permissible branches. Both are along solid boundaries if the west direction is excluded, otherwise one is along the equator oriented to the west. Notice that the Amazon outflow region falls into case III since the coastline is open to the east, and boundary currents are permissible to both north and south of the river mouth.

In cases when only one boundary layer is permissible, obviously all the transport will divert into this boundary

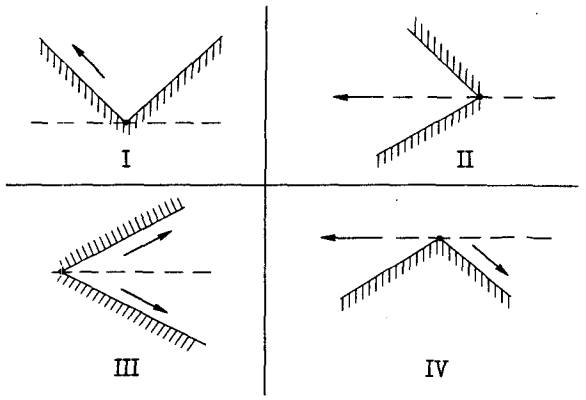

FIG. 2. Examples of four possible arrangements of boundary currents (indicated by thick arrows) for different orientation of the radial boundaries.

layer in the far field. Less trivial are the cases when branching is possible. The question is: How does the transport partition between the two branches? To answer this question, let us examine the symmetry of Eq. (2.2) in the far field. Since in the far field, flow is significant only in the boundary layer where the cross-stream scale is small compared with the alongstream scale, we shall neglect the r derivatives in (2.2) to arrive at the approximate balance (in terms of the radial velocity $u \equiv -r^{-1}\psi_\theta$),

$$u_\theta - r \sin\theta u = 0. \tag{2.7}$$

The equation obviously needs to be modified within the equatorial guide in accordance with earlier scaling analysis, which however does not alter the following symmetry argument. The solution to (2.7) is $u = C \exp(-r\cos\theta)$ where C is a constant determined by the requirement that the total transport is unity. It is seen that, because of the symmetry of the beta effect acting on the flow field, which is subjected only to an integral constraint, the radial flow is symmetric about the equator. Thus a boundary can support significant flow only if its image across the equator (if lying in the open domain) allows such flow. One therefore deduces that for case IV when a free westward jet is permissible, it will dominate the discharge pattern, and for case III when both boundaries allow boundary currents, the one that deviates more from the east direction eventually will siphon all the transport from the other branch in the far field.

For verification of the above results and for visualizing the flow field, I have solved (2.2) numerically using the direct method of Lindzen and Kuo (1969). I have set ψ to the analytical solution (2.3) at $r = 0$ and used the approximate condition $\psi_r = 0$ at the outer boundary $r = r_{max}$. For the numerical solution presented in Fig. 3, r_{max} is chosen to be 5 which is found to be sufficiently large that the solution does not vary significantly for greater r_{max}. In Fig. 3a, as one has expected, the discharge pattern is completely dominated by a westward flow although the solid boundary facing east also allows a boundary layer. The westward flow broadens downstream, consistent with scaling analysis. In Fig. 3b, a straight coast is rotated only slightly (20 deg) from the meridional direction, and one notices the acute asymmetry developed in the discharge pattern even very close to the point source. In Fig. 3c, the geometry is similar to that near the Amazon outflow reigon. One observes that along the central axis, about 80% of the transport has deflected to the northern boundary by a unit distance from the point source. If we use estimates of $\beta \approx 2 \times 10^{-13}\ s^{-1}\ cm^{-1}$ and $C_d \approx 2 \times 10^{-3}$ (Csanady 1982), $U \approx 10\ cm\ s^{-1}$, $H \approx 100$ m so that $\alpha \approx 2 \times 10^{-6}\ s^{-1}$, this unit distance is 100 km. Thus the bulk of the deflection occurs over the shelf proper and may not be strongly influenced by the offshore North Brazil Current.

3. Lateral friction

One might inquire how the use of lateral friction would affect the above results. Using $(\nu/\beta)^{1/3}$ as the spatial scale with ν being the coefficient of kinematic viscosity, the vorticity equation considered is

$$\nabla^4\psi - \cos\theta\psi_r + r^{-1}\sin\theta\psi_\theta = 0, \tag{3.1}$$

where the lateral diffusion of relative vorticity (the first term) is balanced by the advection of planetary vorticity (the remaining terms). The additional boundary conditions need to be imposed are that the solid boundaries are nonslip. The analysis presented below parallels that of the bottom friction case.

In the near field where the beta terms are negligible, (3.1) has the solution

$$\psi = \tfrac{1}{2} + A\sin 2(\theta - \theta_c) + B(\theta - \theta_c), \tag{3.2}$$

where $A = \frac{1}{2}(\Delta\theta\cos\Delta\theta - \sin\Delta\theta)^{-1}$, $B = -2A\cos\Delta\theta$, $\Delta\theta \equiv \theta_2 - \theta_1$, and $\theta_c \equiv \frac{1}{2}(\theta_2 + \theta_1)$. The solution (3.2) no longer represents a uniform radial outflow but contains more structure. For example, it's trivial to see that counterflow is generated when the open angle spanned by the two radial boundaries is greater than 180 degrees.

In the far field, for a nonzonal boundary, the angular spread (θ') of the boundary current still varies as r^{-1}, and with similarity variable η defined as $r\theta'(\sin\theta_b)^{1/3}$, the vorticity equation (3.1) becomes approximately

$$\psi_{\eta\eta\eta\eta} + \psi_\eta = 0, \tag{3.3}$$

which has decaying solution satisfying the required boundary conditions only for negative η (Munk 1950). Thus, as in the previous case, the boundary layer is permissible only on the anticyclonic side of a solid boundary and the current structure is modified just like how Munk's solution (1950) modifies that of the Stommel's (1948).

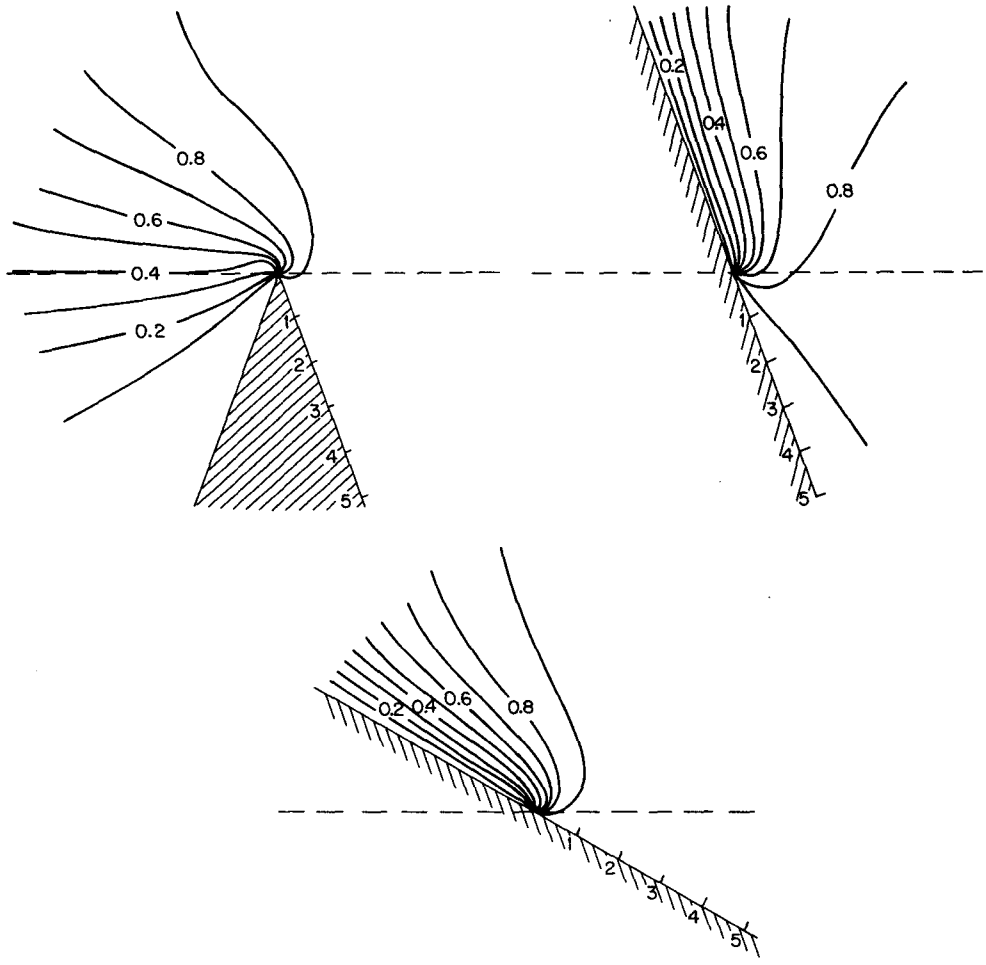

FIG. 3. Numerical solutions for the case of bottom friction for three different model geometry. The orientations of the two radial boundaries (θ_1, θ_2) are: (a) (−70°, 250°), (b) (−70°, 110°), and (c) (−30°, 150°).

If the boundary is zonal, (3.1) implies that θ' decreases at a faster rate ($r^{-3/4}$) than that for the bottom friction case ($|\theta'| \approx r^{-1/2}$). Defining the similarity variable η as $\theta' r^{3/4}$, the similarity solution $\psi(\eta)$ satisfies the equation

$$\psi_{\eta\eta\eta} \mp \frac{1}{4}\eta\psi_\eta = 0, \tag{3.4}$$

where the upper and lower signs are for the boundaries directing to the west and east respectively. As discussed by Gill and Smith (1970), analytical solutions to (3.4) decaying with $|\eta|$ exist only if the upper sign is chosen or, as in the bottom friction case, the boundary current is directed toward the west.

To examine the symmetry of (3.1) in the far field, we again set all r derivatives of ψ to zero to arrive at

$$\psi_{\theta\theta\theta} + 4\psi_\theta + r^3 \sin\theta\psi_\theta = 0, \tag{3.5}$$

or, in terms of the radial flow,

$$u_{\theta\theta} + 4u_\theta + r^3 \sin\theta u = 0. \tag{3.6}$$

Although the equation is invariant to the transformation $\theta \to -\theta$, $u \to u$, the imposition of the no-slip condition upsets the symmetry unless the two boundaries are exact mirror images across the equator. Nevertheless, one can still argue that since the flow is increasingly confined (in its angular spread) as r increases, within which the no-slip conditions are accomodated, the flow outside the boundary layers should still retain some degree of symmetry in the far field. This is supported by a numerical solution of (3.6) shown in Fig. 4. One thus expects the earlier results regarding the partition of the total discharge between branches to remain essentially valid, i.e. the discharge is strongly favored toward the branch that deviates more from the east direction. It is also of interest to note from Fig. 4 that, in contrast to the bottom friction case, counterflows are generated that can reverse the radial flow along some boundaries.

I have also solved (3.1) numerically using the direct method, which involves inverting a large square matrix of a dimension given by the total number of grid points inside the model domain. For the boundary conditions in r, I have set ψ to the analytical solution (3.2) at $r = 0$ and to the numerical solution of (3.5) at the outer

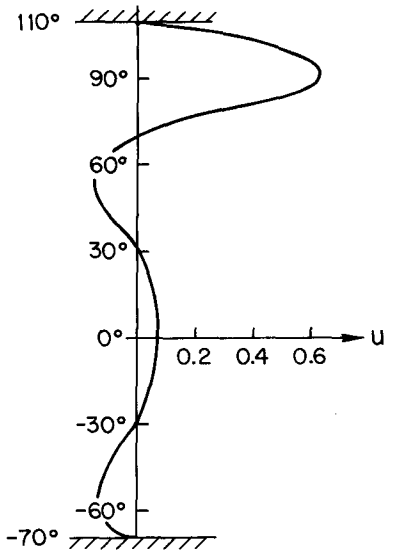

FIG. 4. The numerical solution to (3.5), in terms of the radial velocity, for the case of $(\theta_1, \theta_2) = (-70°, 110°)$ and $r = 5$.

boundary $r = r_{max}$ (together with the supplementary conditions that $\psi_r = \psi_{rr} = 0$). The far-field solution is not accurate near the equatorial guide according to earlier scaling analysis, but it is not expected to change general flow features. I have set $r_{max} = 5$, the adequacy of which has been checked by varying r_{max} to assure that the flow field is not significantly altered. I have also used an iteration method (Roache 1972) to solve (3.1) and found it unsatisfactory for numerical convergence in most cases.

Numerical solutions of (3.1) corresponding to the bottom friction cases of Fig. 3 are plotted in Fig. 5. It is seen that the discharge pattern is similar to the bottom friction case, thus reinforcing the basic conclusion that the discharge will sharply deflect to the boundary (including the equatorial guide) that deviates the most from the east direction. From Fig. 5b, it is seen that the counterflow generated in the far field (see also Fig. 4) penetrates to very near the point source so that the flow is directed toward the north almost along the whole coastline. In all cases, one cannot detect a significant boundary current along the less favorable boundaries.

4. Conclusions

It is seen that whether bottom or lateral friction dominates the dissipation, the discharge pattern is similar and clearly demonstrates the powerful constraint imposed by the beta effect—namely, the discharge is

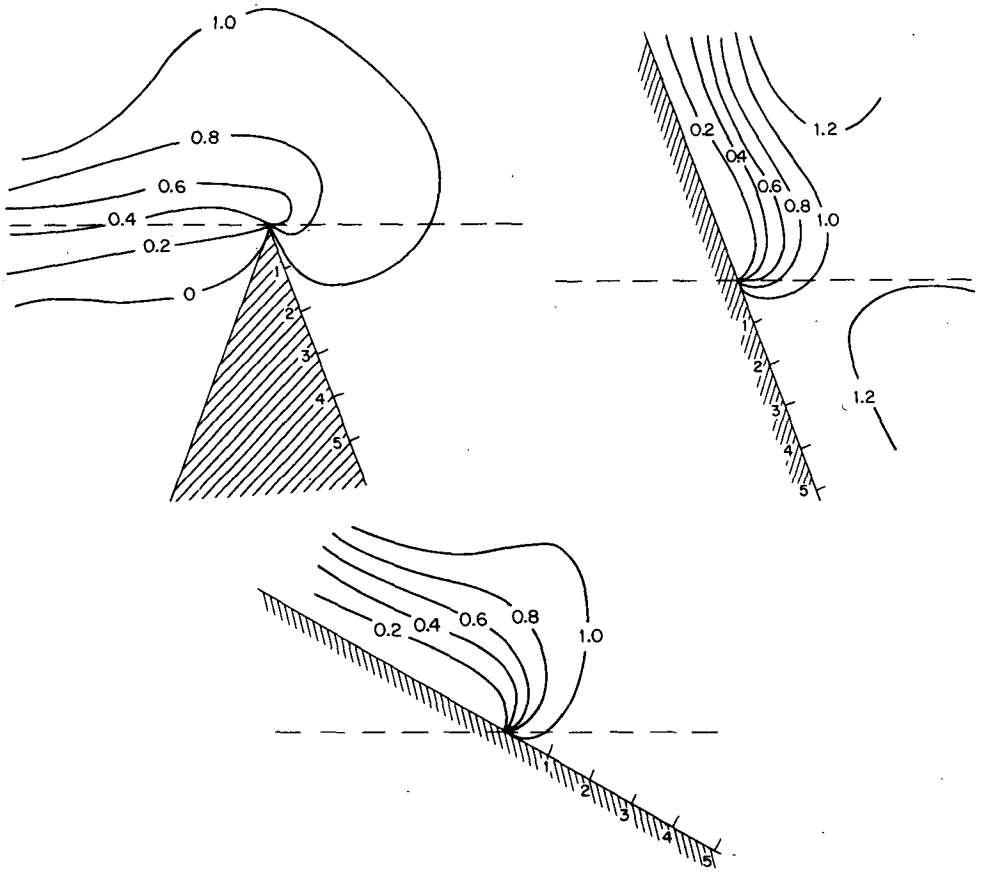

FIG. 5. As in Fig. 3, but for the case of lateral friction.

strongly favored to flow along the boundary (including the equatorial guide to the west of the point source) that deviates the most from the east direction. When both solid boundaries flanking the point source allow boundary layers such as the case when they are open to the east, even a slight asymmetry of their orientation about the equator results in a dramatic redistribution of the discharge, within one frictional scale from the point source. Since, crudely estimated, this scale can be of order 100 km, the model can explain the sharp deflection of the Amazon outflow to the northern coast over the shelf without requiring asymmetric external forcings.

Acknowledgments. I want to thank M. Cane and S. Zebiak for useful discussions, and many of my colleagues for comments leading to improvement of the paper. The work is supported by the National Science Foundation through Grant OCE87-17113.

REFERENCES

Borstad, G. A., 1982: The influence of the meandering Guiana Current and Amazon River discharge on surface salinity near Barbados. *J. Mar. Res.*, **40,** 421–434.

Csanady, G. T., 1982: *Circulation in the Coastal Ocean.* Reidel, 279 pp.

Gibbs, R. J., 1982: Currents on the shelf of Northeastern South America. *Estuar., Coastal Shelf Sci.*, **14,** 283–299.

Gill, A. E., and R. K. Smith, 1970: On similarity solution of the differential equation $\psi_{zzzz} + \psi_x = 0$. *Proc. Camb. Phil. Soc.*, **67,** 163–171.

Lindzen, R. S., and H. L. Kuo, 1969: A reliable method for the numerical integration for a large class of ordinary and partial differential equations. *Mon. Wea. Rev.*, **96,** 732–734.

Muller-Karger, F. E., C. R. McClain and P. L. Richardson, 1988: The dispersal of the Amazon's water. *Nature,* **333,** 56–59.

Munk, W. H., 1960: On the wind-driven ocean circulation. *J. Meteor.*, **7,** 79–93.

Roache, P. J., 1972: *Computational Fluid Dynamics.* Hermosa, 446 pp.

Stommel, H., 1948: The westward intensification of wind-driven ocean currents. *Trans. Am. Geophys. Union,* **29**(2), 202–206.